Available online at www.sciencedirect.com
SCIENCE DIRECT
International Journal of Fatigue 27 (2005) 1147–1158
International Journal of Fatigue
www.elsevier.com/locate/ijfatigue

Fatigue behavior of nanocrystalline metals and alloys

T. Hanlon[a,c], E.D. Tabachnikova[b], S. Suresh[a,*]

[a]Department of Materials Science and Engineering, Massachusetts Institute of Technology, Cambridge, MA 02139, USA
[b]B. Verkin Institute for Low Temperature Physics and Engineering, National Academy of Sciences of the Ukraine, Kharkov-103, 61103 Ukraine
[c]GE, Global Research Center, Niskayuna, NY 12309, USA

Available online 2 August 2005

Abstract

In this work, the stress-life fatigue behavior and fatigue crack growth characteristics of pure Ni were studied as a function of grain size spanning a range of tens of nanometer to tens of micrometer. The fatigue response of electrodeposited, fully dense, nanocrystalline pure Ni, with average and total range of grain sizes well below 100 nm, was compared and contrasted with that of electrodeposited ultrafine-crystalline pure Ni with an average grain size of about 300 nm and conventional microcrystalline Ni with an average grain size in excess of 10 μm. It was found that grain refinement to the nanocrystalline regime generally leads to an increase in total life under stress-controlled fatigue whereas a deleterious effect was seen on the resistance to fatigue crack growth at low and high tensile load ratio levels. To explore the generality of the above trends, systematic experiments were also performed in ultrafine-crystalline pure Ti produced by equal-channel angular pressing where a reduction in grain size was found to cause an increase in fatigue crack growth rates at different tensile load ratios. Grain refinement from the microcrystalline to the ultrafine-crystalline regime by cryomilling of Al alloys also showed a similar response. Possible mechanistic origins of such trends are explored, and some general conclusions are extracted on strategies for improvements in the fatigue resistance of engineering structures by recourse to grain refinement down to the nanocrystalline regime.

1. Introduction

Control of the resistance of metals and alloys to fracture and fatigue through grain refinement has long been a strategy for improving the structural integrity of engineering components. The vast majority of studies in this area have dealt with microcrystalline (mc) metals and alloys with an average grain size typically larger than 1 μm (see, for example [1]), although a limited amount of experimental information is also available for ultrafine-crystalline (ufc) metals [2–6]. An examination of these studies leads to the following general observations [1,5]. Grain refinement, which leads to the strengthening of mc and ufc metals and alloys, is usually accompanied by an increase in fatigue endurance limit. Consequently, stress-life curves, which provide an indication of the dependence of total fatigue life on cyclic stress in nominally smooth fatigue specimens subjected to constant amplitude cyclic load, generally point to an improvement in fatigue resistance with decreasing grain size. Here the beneficial effect on fatigue life is typically considered to arise from the inhibition of cracks that nucleate at nominally smooth surfaces in response to the higher endurance limit. In contrast to this trend, fatigue damage tolerance generally deteriorates with grain refinement especially at low stress intensity range, ΔK, in the near-threshold regime. This apparent increase in resistance to fatigue fracture with increasing grain size is attributed to possible effects of the lowering of effective driving force from microstructurally induced changes in crack path and the attendant possibility of contact between crack face asperities [7]. This apparently beneficial effect is typically more pronounced at low ΔK levels where the cyclic plastic zone size and the cyclic crack tip opening displacement are smaller than the grain size in mc metals.

The foregoing general trends pertaining to grain size effects of fatigue crack initiation and crack growth have thus far not been assessed fully for the broad spectrum of grain sizes spanning the microcrystalline to the nanocrystalline regime. Indeed, the recent surge in research interest in nanostructured materials has provided valuable insights into the potential benefits and drawbacks of grain refinement in the nanocrystalline (nc) regime, where the grain size is typically smaller than 100 nm, on various mechanical properties [8–11]. However, the role of nanoscale grains

* Corresponding author. Tel.: +1 617 253 3320; fax: +1 617 253 0868.
E-mail address: ssuresh@mit.edu (S. Suresh).

0142-1123/$ - see front matter © 2005 Elsevier Ltd. All rights reserved.
doi:10.1016/j.ijfatigue.2005.06.035

in influencing the resistance to fatigue of engineering metals and alloys has not been explored in sufficient detail, despite the fact that the potential use of nanocrystalline materials in load-bearing engineering structures critically depends on their tolerance to the onset and progression of damage from cyclic loading. One factor contributing to this relative lack of information on the fatigue response of nc materials is the difficulty in producing truly nc metals and alloys (whose average as well as extreme grain dimensions are all smaller than about 100 nm) in sufficiently large quantities to facilitate 'valid' tests that comply with the American Society for Testing and Materials (ASTM) standards for minimum specimen dimensions and small-scale yielding for characterization using linear elastic fracture mechanics (LEFM). In an attempt to circumvent these difficulties, several studies [2–4] have employed ufc metals produced by equal-channel angular pressing (ECAP) to explore grain size effects on cyclic deformation. However, the high initial defect density inherent in these materials significantly biases the fatigue response of the material. Furthermore, such processing methods are not presently amenable to produce truly nc metals in that the microstructure comprises a significantly large fraction of grains whose dimensions exceed 100 nm; these grains typically dominate the overall mechanical response. The only study available to date on the fatigue response of fully nc metals is a preliminary report from the present work [5].

This investigation was initiated with the objective of probing the effects of cyclic loading on the fatigue resistance of fully dense nc metals. The stress-life (S–N) fatigue response and the fatigue crack growth resistance of truly nc electrodeposited pure Ni was assessed, with the crack growth response further examined over a wide range of tensile load ratios. In order to assess the effects of grain size control and grain-boundary engineering on fatigue response, the results obtained for nc Ni are compared with those for ufc and mc metals and alloys, wherever feasible. In order to further assess the broad generality of the conclusions of this study, additional crack growth experiments were also conducted in a cryomilled ufc Al–Mg alloy and an equal channel angular pressed (ECAP) Grade 2 pure Ti, for which sizeable quantities of bulk specimens were available such that conventional fatigue testing could be employed. From these observations, mechanistic interpretations of the effects of grain size on fatigue response are developed, and possible strategies for grain size engineering in damage-critical applications are suggested.

2. Materials and experimental methods

2.1. Model material system

The choice of a model material system, and corresponding fabrication technique, was predicated upon the following requirements: (1) the attainability of a true nc grain structure where the average and the largest grain size are both below 100 nm, (2) the ability to achieve a high level of material purity, with sufficient reproducibility, and (3) the capability to produce a fully dense structure. Such requirements ensure that the material produced can accurately be described as nc. Particular attention was paid to maintaining a range of grain sizes well below 100 nm to avoid having any larger 'outlier' grains dominate the fatigue response.

While there are many methods currently available to fabricate nc materials [12–22], electrodeposited Ni was chosen as the model system for this investigation. It can be produced over a broad range of grain sizes, from the nc to the mc regime, and is capable of satisfying the above-mentioned requirements. Two notable advantages of the electrodeposition process are the ability to produce relatively large (in-plane) quantities of uniform, fully dense material (e.g. 80×80 mm), and the capacity to confine the grain size to a narrow distribution (Fig. 1). Although the attainable thickness resides in the millimeter range, samples in this investigation were purposely limited to a thickness of approximately 100–150 μm, to ensure through-thickness grain size uniformity and to avoid processing induced residual stresses. Electrodeposited Ni foils with two different grain sizes (nc Ni with an average grain size of 20–40 nm and a ufc equi-axed structure with an average grain size of approximately 300 nm) were procured from Integran Corporation, Toronto, Canada.

2.2. Experimental details

For the purpose of minimizing processing-induced residual stresses, all fatigue specimens were extracted from the electrodeposited Ni foils by way of electro-discharge machining. Both low- and high-cycle fatigue

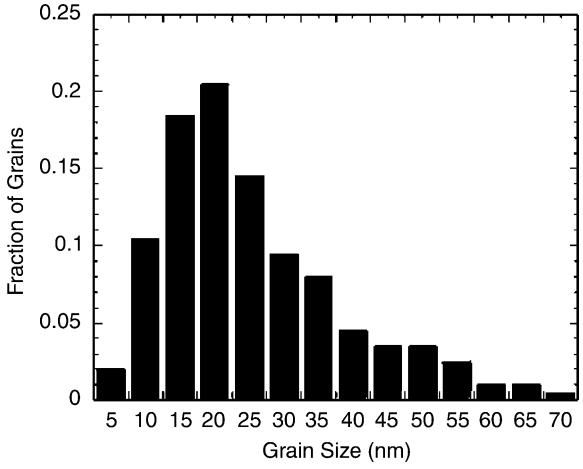

Fig. 1. Grain size distribution of electrodeposited pure nc Ni, illustrating the relatively narrow range of grain sizes, as well as the confinement of all grains below the 100 nm range.

experiments were carried out in a laboratory air environment (approximately 25 °C and 50% relative humidity). Full details of the stress-life set-up and experimental methods are available elsewhere [5,20].

High cycle fatigue crack growth experiments for the nc, ufc, and mc Ni foils were conducted using single edge-notched specimens, where fatigue cracks were initiated in cyclic tension at load ratios ranging from 0.1 to 0.7 at a cyclic frequency of 10 Hz (sinusoidal waveform). The specimens were 39 mm long, 9.9 mm wide, and 100 μm in thickness. Changes in crack length as a function of the number of fatigue cycles were monitored optically with a traveling microscope. The crack growth rate, da/dN, was monitored as the length of the crack increased under a constant range of imposed cyclic loads. To ensure that small-scale yielding conditions prevailed, all data were collected such that the remaining uncracked ligament length was always at least twenty times greater than the maximum plastic zone size at the crack tip.

In order to assess the overall generality of the trends observed in electrodeposited Ni, we studied the fatigue properties of two additional material systems, for which larger bulk specimens could be produced. First, a cryomilled Al-7.5Mg alloy was fabricated in billet form, 50 mm in diameter, and several inches in length (and was procured from the University of California, Irvine). This choice was motivated by the fact that grain size effects could be assessed in the ufc regime using specimens whose dimensions are sufficiently large (35×35×5 mm) to meet the requirements of conventional standards for fatigue testing of bulk materials. A complete review of the Al-7.5Mg powder production and consolidation techniques is given in [23,24]. In addition, ufc, ECAP pure Ti was also investigated, with direct comparisons made to its mc counterpart.

Compact specimens, 5 mm in thickness, were extracted from extruded Al–Mg billets in the circumferential–radial (C–R) configuration. The notch tip was machined to a radius of 0.09 mm and the specimen faces were polished to a mirror finish, with a final 0.25 μm polishing step. The through-holes, located on either side of the notch to pin-load the specimens, were machined after the fatigue pre-crack was introduced via cyclic compression loading [1,25,26]. Full details of the experimental technique are given in [5].

For the study of fatigue of ECAP materials, billets of Grade 2 commercially pure mc Ti, 40 mm in diameter and 150 mm in length, were subjected to eight ECAP cycles at a temperature of 425 °C, using a molybdenum disulphide lubricant and a die angle of 90°. Compact specimens, 3 mm in thickness, were extracted in the radial–longitudinal (R–L) configuration from billets from the same batch exposed to either zero (mc Ti) or eight (ufc Ti) such pressing cycles. In-plane dimensions of the specimens measured 33× 31.75 mm. The notch tip was machined to an initial radius of 0.12 mm, and subsequently sharpened to a radius of 0.03 mm with a razor blade sprayed with a 0.25 μm diamond polishing suspension. A fatigue pre-crack was introduced in cyclic tension at load ratios of $R=0.1$ and 0.3, at a cyclic frequency of 10 Hz (sinusoidal waveform) at room temperature. Crack growth was monitored in-situ with a telescopic video camera module, and ex-situ with an optical microscope.

2.3. Shape factor considerations

In order to characterize the variation of the fatigue crack growth rate as a function of ΔK, a proper evaluation of the shape factor, $f(a/W)$, specific to the present specimen geometry (single-edge-notched tension specimen) and loading configuration was required. For a rectangular plate of width, W, containing a through-thickness edge crack of length, a, it is commonly known that the stress intensity factor can be expressed by:

$$K_{\mathrm{I}} = \sigma\sqrt{a} f\left(\frac{a}{W}\right), \quad f\left(\frac{a}{W}\right) = 1.99 - 0.41\left(\frac{a}{W}\right) + 18.7\left(\frac{a}{W}\right)^2 - 38.48\left(\frac{a}{W}\right)^3 + 53.85\left(\frac{a}{W}\right)^4 \tag{1}$$

However, the above expression is limited to loading configurations capable of producing a *uniform* stress throughout the specimen. Typically, this can be accomplished by utilizing proper sample geometry (i.e. height, $H>2W$). Eq. (1) must be modified when a non-uniform stress is applied.

In order to conduct experiments at a sufficiently high frequency, it was necessary to load the edge-notch specimens using rigid, as opposed to pin-loaded grips. In the latter, there exists a rotational degree of freedom, which produces an opening moment at the crack tip during tensile loading. Upon loading with such grips, a significant degradation of the imposed sinusoidal waveform occurred at approximately 3–5 Hz. This was accompanied by machine resonance, which rendered the system unstable. Conversely, when the specimens were loaded with rigid grips (i.e. 'fixed end displacement' loading), where the ends of the specimens were displaced by a constant amount, a clean sinusoidal waveform at the desired frequency of 10 Hz was easily achieved.

Several authors [27–30] have previously recognized that the application of Eq. (1) to a fixed-end displacement loading configuration can substantially overestimate the mode I stress intensity factor. The boundary conditions associated with this type of loading are such that a closing bending moment is imposed on the crack, even during tensile loading, due to the lack of rotational freedom in the grips. This imposed closing moment effectively reduces the stress intensity factor, and therefore the driving force for crack propagation.

To account for this relative reduction in ΔK, the shape factor, $f(a/W)$, was evaluated via finite element analysis for

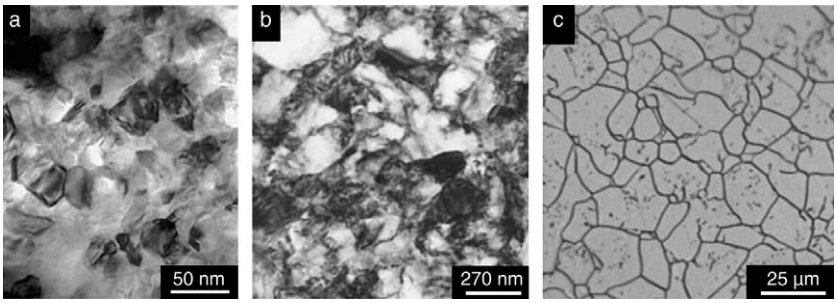

Fig. 2. Electron and optical micrographs of the (a) nc Ni, (b) ufc Ni, and (c) mc Ni investigated [5].

the specific loading geometry used in this investigation. In the analysis, the J-integral was calculated for a/W values ranging from 0.1 to 0.7, fully encompassing the range investigated experimentally. Assuming that the stress intensity factor, K_I, has the form given in Eq. (1), the shape factor can be expressed as follows:

$$f\left(\frac{a}{W}\right) = \sqrt{\frac{JE}{a\sigma^2}} \tag{2}$$

where E is Young's modulus and the relationship in Eq. (2) pertains to plane stress conditions. By applying a prescribed load, J can be systematically solved for over a range of crack lengths. In this manner, the shape factor can be fully characterized for the loading configuration and specimen geometry of interest.

To confirm the accuracy of the analysis, a constant stress loading configuration was modeled, and the resulting shape factor was found to compare well with the standard formula given in Eq. (1). Eq. (3) specifies the shape factor determined from the analysis (detailed descriptions of which can be found in Ref. [20]) for the fixed end displacement case, which was employed in all calculations of the stress intensity factor used to interpret the fatigue crack growth results.

$$f\left(\frac{a}{W}\right) = 2.03 - 0.43\left(\frac{a}{W}\right) + 3.96\left(\frac{a}{W}\right)^2 - 6.04\left(\frac{a}{W}\right)^3 + 5.68\left(\frac{a}{W}\right)^4 \tag{3}$$

3. Results

3.1. Structure and tensile properties

Specimens of nc and ufc Ni were fully characterized in their as-received state by recourse to electron microscopy (Fig. 2) and/or x-ray diffraction. The electrodeposited nc Ni had a columnar grain structure with an aspect ratio of 7–10, whereas the electrodeposited ufc Ni was nearly equiaxed. The micrographs in Fig. 2a,b depict relatively defect-free initial structures, a critical factor in assessing the role of grain size on the overall fatigue response. Full details of the electrodeposition process and resulting Ni structure are reported elsewhere [14,31,32].

Tensile testing of nc and ufc Ni specimens revealed 0.2% offset yield strength values of 930 and 525 MPa, respectively, and strain to failure values of 3 and 10%, respectively. The mc Ni had a yield strength of 180 MPa, tensile strength of 450 MPa and tensile strain to failure of 35%.

Transmission electron microscopy (TEM) images show that the Al–Mg alloy investigated has a relatively equiaxed grain structure, with an average grain size of ~300 nm [24]. Its yield and tensile strengths were measured experimentally to be 540 and 551 MPa, respectively. The structure of the ufc ECAP Ti was also relatively equiaxed, with an average grain size of approximately 250 nm (Fig. 3) and a yield strength of 635 MPa. Image analysis of the mc Ti revealed an average grain size of ~22 μm, while its yield strength was measured at 430 MPa. Full processing and property details are reported in [33].

3.2. Fatigue response

3.2.1. Stress-controlled fatigue

The effect of grain size on the fatigue resistance of initially smooth-surfaced pure Ni is shown in Fig. 4 in the form of stress-life fatigue curves, from our earlier report [5]. It is evident that nc Ni has a slightly (and reproducibly) higher resistance to stress-controlled fatigue loading than ufc Ni. Additionally, the endurance limit of the mc Ni is significantly below that of both the nc and ufc material,

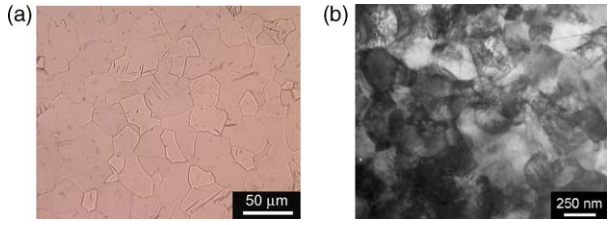

Fig. 3. (a) Optical micrograph showing the grain size distribution of the Grade 2 pure mc Ti investigated (zero pressing cycles). (b) TEM image of the ufc ECAP Ti, subjected to 8 pressing cycles at a temperature of 425 °C.

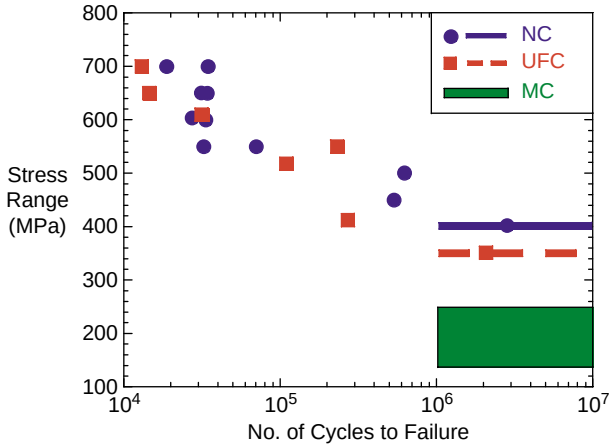

Fig. 4. The effects of grain size from the micro to the nano-regime on the cyclic stress vs. total number of cycles to failure plot in pure Ni. (From [5]).

clearly illustrating the beneficial effects of grain size reduction on the resistance to S–N fatigue.

3.2.2. Fatigue crack growth

The variation in fatigue crack growth rate with respect to ΔK for pure Ni at load ratios of $R=0.1$, 0.3, and 0.7 is plotted in Fig. 5. In order to enforce the assumptions inherent to LEFM, all data collection was truncated to incorporate only those data points corresponding to an uncracked ligament length of at least 20 times the plastic zone size at the tip of the crack during fatigue crack growth experiments. Due to the relatively limited strength of mc Ni, valid fatigue crack growth experiments using ΔK as the characterizing parameter were not possible under the abovementioned requirements. It is evident from Fig. 5 that the resistance to fatigue crack growth is substantially lower in nc Ni at all levels of applied loading, over a wide range of load ratios.

To circumvent the foregoing issues associated with the extent of crack-tip plasticity, a set of data was also collected relating the change in crack length to the number of fatigue cycles in mc, ufc, and nc Ni (Fig. 6). Each material was subjected to identical initial loading conditions of $\Delta K=9.5$ MPa $m^{1/2}$, $R=0.3$, and a cyclic frequency of 10 Hz at room temperature. Fig. 6 clearly illustrates that the crack growth rate in the nc Ni is significantly higher than that in the ufc and mc Ni. The effects of load ratio R on the fatigue crack growth response in nc and ufc Ni are plotted in Fig. 7, where an increase in R leads to faster crack growth in both materials over the entire range of ΔK examined. These results are replotted in Fig. 8 where the stress intensity factor range ΔK required for a growth rate of 10^{-6} mm per

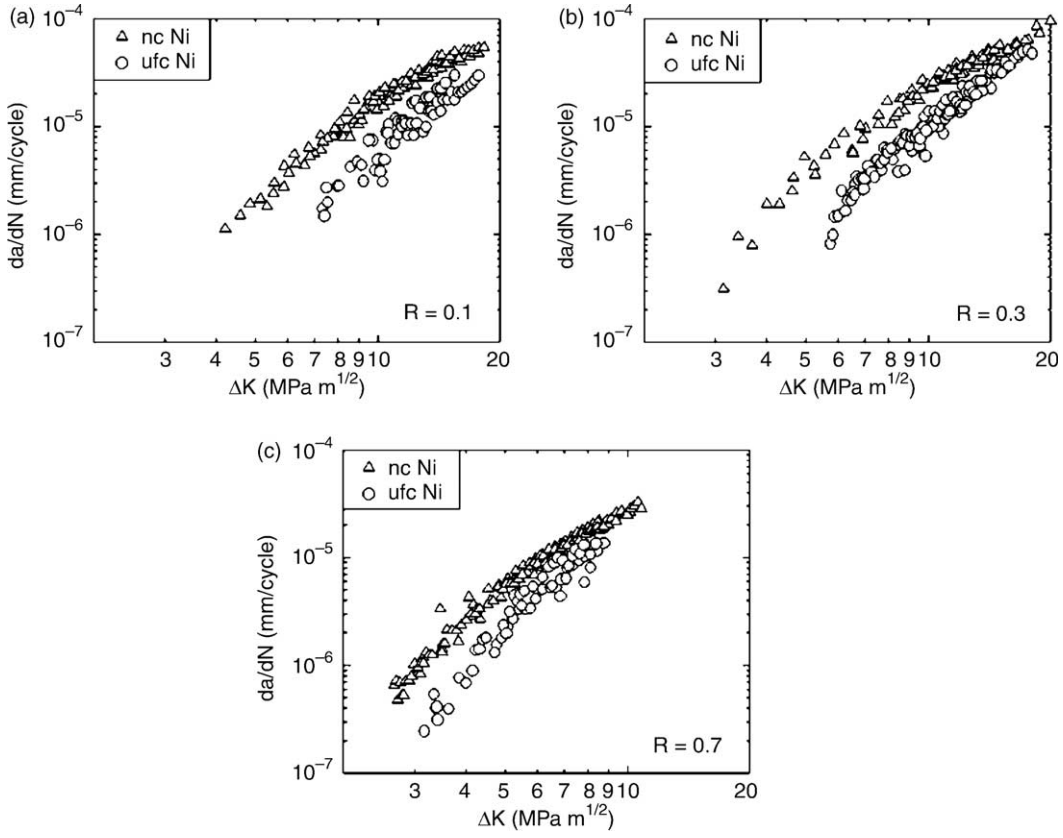

Fig. 5. Variation of the fatigue crack growth rate, da/dN, as a function of ΔK for pure electrodeposited ufc, and nc Ni at load ratios (a) $R=0.1$, (b) $R=0.3$, and (c) $R=0.7$, at a fatigue frequency of 10 Hz at room temperature.

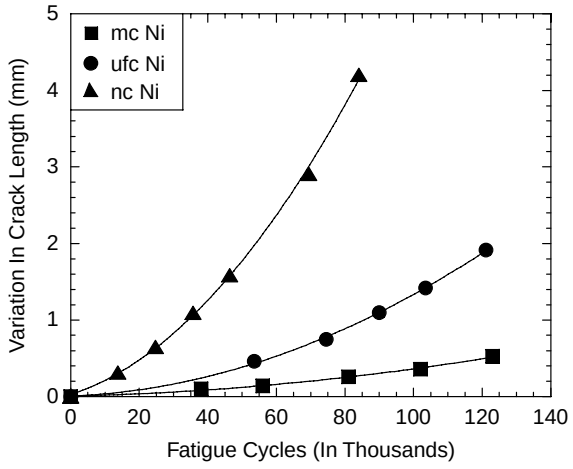

Fig. 6. Variation in crack length as a function of the number of imposed fatigue cycles for mc, ufc, and nc Ni subjected to an initial ΔK of 9.5 MPa $m^{1/2}$, load ratio $R=0.3$, and cyclic frequency of 10 Hz at room temperature.

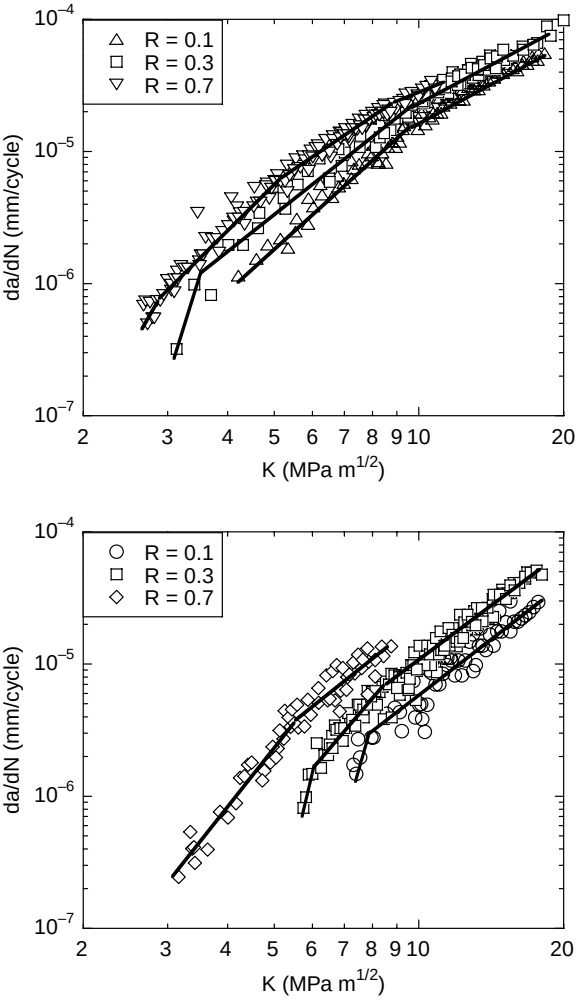

Fig. 7. Fatigue crack growth rate as a function of ΔK at different load ratios for nc Ni (upper figure) and ufc Ni (lower figure).

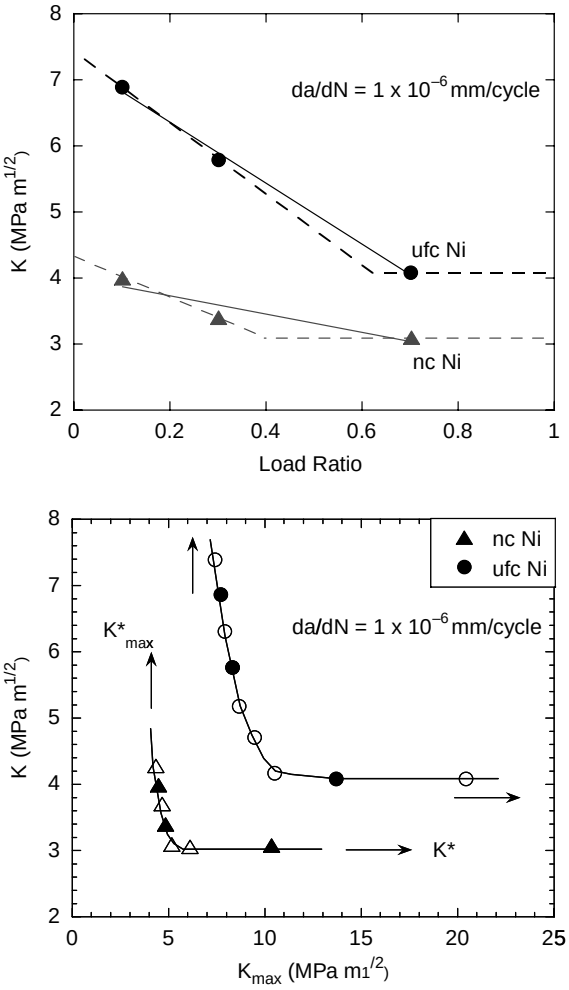

Fig. 8. Stress intensity factor range ΔK required to induce a growth rate of 10^{-6} mm per cycle in nc and ufc Ni is replotted from the information in Fig. 7 as a function of R (top figure) and maximum stress intensity factor range, K^*_{max} (bottom figure). The solid lines in both figures show actual trend lines whereas the dashed lines denote assumed trends. Here it is assumed that there exists a critical R above which crack growth is unaffected by R. The filled symbols in the latter figure are experimental data and the open symbols are interpolated points extracted from the information given in the upper figure. ΔK^* and K^*_{max}, respectively, denote the limiting or threshold values of alternating and maximum values of stress intensity factor required for the particular growth rate of 10^{-6} mm per cycle. These values increase with increasing crack growth rate. The apparently detrimental effect of grain refinement on crack growth is evident in both figures.

cycle in nc and ufc Ni is plotted as a function of R and maximum stress intensity factor, K_{max}. The deleterious effect of grain refinement on crack growth is evident in this figure. Further, discussion of the trends seen in this figure is taken up in a later section.

To further explore the validity and generality of the above fatigue crack growth trends to fine-grained metals and alloys produced by other processing methods, additional ufc materials fabricated via cryomilling (ufc Al-7.5Mg) and equal channel angular pressing (ufc pure Ti), for which larger bulk specimens could be procured, were examined. Since the solid solution Al-7.5Mg alloy

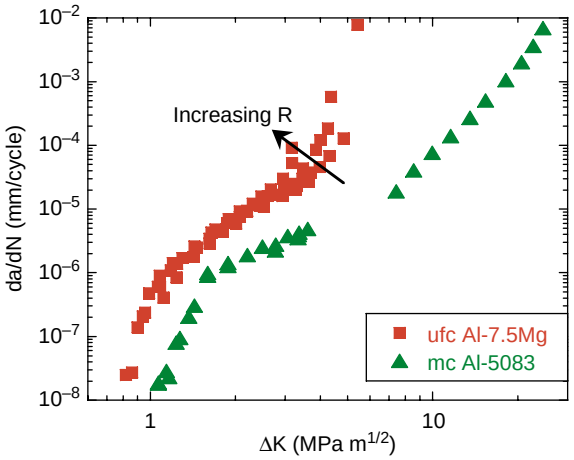

Fig. 9. Variation of the fatigue crack growth rate, da/dN, as a function of the stress intensity factor range, ΔK, for ufc cryomilled Al-7.5Mg at $R=0.1$–0.5 at a fatigue frequency of 10 Hz at room temperature. Also shown are the corresponding crack growth data for a commercial mc 5083 aluminum alloy at $R=0.33$ [14].

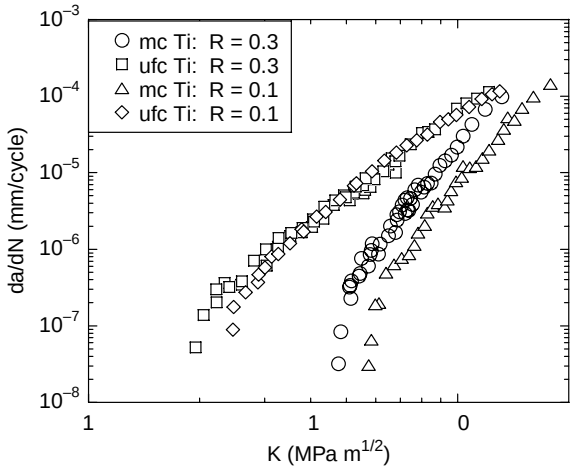

Fig. 10. Variation in fatigue crack growth rate as a function of ΔK for commercially pure mc Ti and ECAP ufc Ti at a fatigue frequency of 10 Hz at room temperature.

could only be fabricated via cryomilling, which ultimately results in a very fine grain structure, a direct comparison to mc Al-7.5Mg could not be made. However, Al-5083 is a close mc counterpart, and is often used for comparison purposes [24].

Consistent with the results obtained for electrodeposited Ni, it was found that the ufc Al-7.5Mg fatigue crack growth rates over the entire da/dN range, from threshold to final failure, were substantially higher than those in the mc Al-5083 (Fig. 9). The threshold stress intensity factor range was also considerably lower in the ufc material. In addition, the critical value of ΔK at which catastrophic failure occurred was several times smaller in the cryomilled Al–Mg. Examination of the fracture surface of the ufc material revealed a significant amount of cracking at inclusion particles [5], which were likely introduced during the cryomilling process. Such particles are believed to play a significant role in the lowering of the critical value of ΔK.

Fatigue crack growth response of pure mc and ECAP-processed ufc Ti was also fully characterized from threshold to final failure. Fig. 10 shows effects of grain size on the variation of da/dN as a function of ΔK at load ratios of $R=$ 0.1 and 0.3. Here, grain refinement from the mc to the ufc regime leads to a reduction in ΔK_{th} by a factor of 2.5. The rate of fatigue crack propagation is more than an order of magnitude higher in the ufc Ti, over a wide range of applied loading, further reflecting the same trends captured in the electrodeposited Ni.

4. Discussion

Studies of fatigue crack initiation in microcrystalline metals and alloys have long considered the critical role of purity, surface preparation and material strength in influencing the stress-life response. In nominally smooth-surfaced and defect-free fatigue specimens without notches and other stress concentrators, the initiation of cracks is known to occur in high-cycle fatigue at surfaces. An increase in the strength and hardness of the material, especially near the surface regions which serve as crack nucleation sites, is therefore considered to impart a greater resistance to fatigue crack initiation and hence to S–N fatigue. In the present experiments involving pure Ni and smooth laboratory specimens, this trend is seen to extend down to the nanocrystalline regime, where the higher strength and hardness of the nc material serves to provide a greater resistance to high cycle fatigue than the ufc and mc Ni.[1]

Prior work on the fatigue crack growth resistance of conventional mc metals and alloys has shown (see, for example, [1] for a review of the literature) that predominantly crystallographic and stage I crack growth mechanisms arising at low ΔK levels of fatigue crack growth lead to microstructurally tortuous crack paths in the coarser grained materials. Grain refinement in mc alloys then serves to reduce the extent of such crack path tortuosity, especially in the near-threshold regime where the cyclic plastic zone size is typically smaller than the average grain size and where the maximum crack-tip opening displacement can be markedly smaller than the surface asperity dimension. These seemingly small periodic deflections in the path of the crack can lead to changes in effective ΔK as a result of the net reduction in the local stress intensity factor range compared to the case of a perfectly straight crack front [7]. In addition, when the

[1] Nanocrystalline metals produced by electrodeposition are known to contain hydrogen which is introduced during processing. However, in the present work, the effects of such impurities are not found to play a major role in introducing damage in nc Ni, as corroborated through high-resolution transmission electron microscopy [31].

average crack growth rate is measured only in a direction normal to the cyclic tension-loading axis, periodic deflections in the crack path lead to an apparently smaller rate of crack growth (at the same effective driving force as that experienced by a perfectly straight fatigue crack in the same material). In addition to these two geometric effects, the irreversibility of cyclic slip directly ahead of the fatigue crack tip (for example, that induced by the oxidation of slip steps) can lead to overall mode II displacements and hence mismatch between mating crack face asperities immediately behind the crack tip [1,7]. This 'partial closure' effect can be exacerbated by the periodic deflections in crack path. A consequence of such a mismatch between asperities is that it can lead to a further reduction in the effective driving force for fatigue fracture (at the same nominal far-field cyclic loading) and an apparently lower rate of fatigue crack growth. The collective effect of all these factors is that coarser grained mc metals and alloys exhibit apparently greater resistance to subcritical fatigue fracture than finer grained ones.

In the present study involving fatigue crack growth in Ni, it is evident that decreasing the grain size from the mc to the ufc to the nc regime leads to a remarkable reduction in the extent of crack path tortuosity and fracture surface roughness. Fig. 11 shows that the fatigue crack paths emerging in mc and ufc Ni are crystallographic with the extent of crack face roughness significantly diminishing from the mc to the ufc grain size. This smoothening of fatigue fracture surface would be expected to be even more pronounced with grain refinement from the ufc to the nc regime, irrespectively of whether the nc material undergoes fatigue fracture by an intergranular or transgranular separation mechanism. Fig. 11 shows the significantly straighter fatigue fracture path in nc Ni compared to the other two grain size conditions.

Under small-scale yielding conditions and plane stress, the crack tip opening displacement can be expressed as:

$$\delta_{\max} = d_n \frac{K_{\max}^2}{\sigma_y E} \tag{4}$$

where $\delta_{\max}$ is the maximum opening displacement at the tip of the crack, d_n is a constant which is strongly influenced by the strain hardening exponent, n, σ_y is the yield strength, and E is the Young's modulus of the material. d_n typically varies between 0.3 and 0.8 as n is increased from 3 to 13 [34]. Assuming a value of $d_n = 0.8$, the maximum crack tip opening displacements calculated for the samples in Fig. 11a–c are 3.6, 0.60, and 0.63 μm, respectively. The height of the corresponding surface asperities in mc and ufc Ni is approximately 10 and 5.2 μm, respectively. Because the fracture surface asperities are significantly larger than the respective maximum crack tip opening displacements in both the mc and ufc Ni specimens, premature contact between the mating crack face asperities (especially those immediately behind the crack tip) would be expected to influence the fatigue crack growth rate in these materials, even if there is a only a very small amount of mismatch or overall mode II displacement. Conversely, the maximum measurable surface asperity height in the nc Ni (Fig. 11f) was well below the corresponding $\delta_{\max}$. In addition, there was no substantial crack deflection observed in the nc Ni.

Under nominally mode I fatigue loading, any deviation of the crack away from the mode I growth plane leads to mixed mode loading conditions locally at the tip of the crack. When a fatigue crack propagating in the pure mode I plane uniformly kinks at an inclined angle, θ, with respect to the mode I plane, the local mode I and mode II stress intensity factors, k_1 and k_2, are:

$$\begin{aligned} k_1 &= \frac{1}{4}\left(3\cos\frac{\theta}{2} + \cos\frac{3\theta}{2}\right)K_{\mathrm{I}} - \frac{3}{4}\left(\sin\frac{\theta}{2} + \sin\frac{3\theta}{2}\right)K_{\mathrm{II}} \\ k_2 &= \frac{1}{4}\left(\sin\frac{\theta}{2} + \sin\frac{3\theta}{2}\right)K_{\mathrm{I}} + \frac{1}{4}\left(\cos\frac{\theta}{2} + 3\cos\frac{3\theta}{2}\right)K_{\mathrm{II}} \end{aligned} \tag{5}$$

where K_{I} and K_{II} represent the global mode I and mode II stress intensity factors, and the bracketed coefficients are dimensionless factors reported by [35,36]. Under pure mode

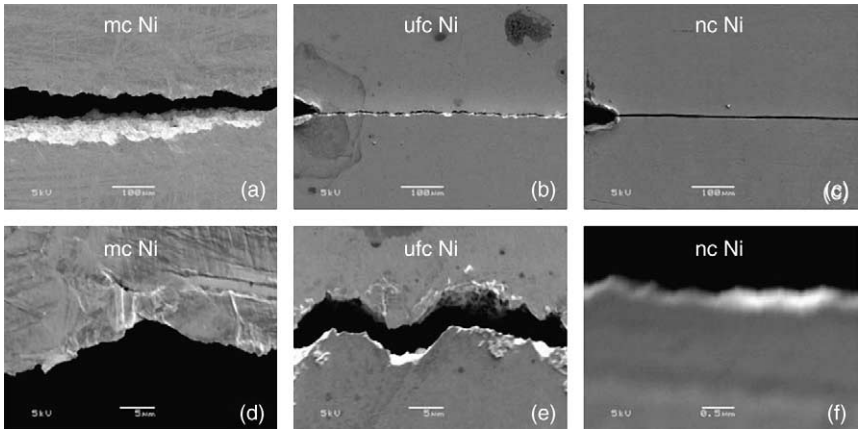

Fig. 11. Scanning electron micrographs of mc, ufc, and nc Ni subjected to sinusoidal fatigue loading at initial ΔK values of 10, 6.2, and 8.5 MPa $m^{1/2}$, respectively. A cyclic frequency of 10 Hz and load ratio, $R = 0.3$ were used in all cases. Crack path tortuosity clearly decreases with grain refinement. Images (d) through (f) are higher magnification images of (a) through (c), respectively, and the magnification of (f) is 10 times that of (d) and (e).

I far field loading conditions, the second term in each equation vanishes, and k_1 and k_2 become

$$k_1 = \cos^3\left(\frac{\theta}{2}\right)K_I \quad k_2 = \sin\left(\frac{\theta}{2}\right)\cos^2\left(\frac{\theta}{2}\right)K_I \tag{6}$$

The local effective stress intensity factor at the tip of the crack is then approximated by the geometric sum of k_1 and k_2.

$$k_{eff} = \cos^2\left(\frac{\theta}{2}\right)K_I \tag{7}$$

Eq. (7) clearly demonstrates that deflection alone reduces the driving force for crack propagation.

Full details of a model that captures the effects of deflection and closure in periodically deflected cracks is reported elsewhere [7]. Here, the repeating unit in a periodically deflected fatigue crack is assumed to comprise a nominally straight segment of length S, oriented perpendicular to the global mode I loading axis, and a kinked segment, of length D, inclined at an angle, θ. Because the surfaces of a crack do not generally mate perfectly during the unloading phase of a fatigue cycle if there exists even a small mismatch or mode II displacement, some level of premature locking of crack-face asperities is normally anticipated. The level of mismatch between the fracture surfaces at the onset of contact during unloading, χ, is characterized by the ratio of in-plane (u_{II}) to normal (u_I) displacement of the crack faces [7].

$$\chi = \frac{u_{II}}{u_I} \tag{8}$$

Taking the weighted average of the effective stress intensity factor for the kinked crack, Eq. (7), and the straight crack, and imposing the effects of mismatch, the ratio of the global and local effective stress intensity factor ranges are found to be [7]:

$$\frac{\Delta K_I}{\Delta k_{eff}} \approx \left(\frac{D\cos^2\left(\frac{\theta}{2}\right)+S}{D+S}\right)^{-1}\left(1-\left[\frac{\chi\tan\theta}{1+\chi\tan\theta}\right]^{1/2}\right)^{-1} \tag{9}$$

Because crack length is generally measured along the axis perpendicular to the applied loading, deflected cracks appear to grow at a different rate than those that are undeflected, under equivalent values of Δk_{eff}. To account for the extra crack length accrued during deflection, the linear undeflected crack growth rate $(da/dN)_L$ must be modified as follows [7]:

$$\left(\frac{da}{dN}\right) = \left(\frac{D\cos\theta+S}{D+S}\right)\left(\frac{da}{dN}\right)_L \tag{10}$$

Eqs. 9 and 10 can be used to predict the rate of crack growth as a function of ΔK for tortuous crack paths, assuming that the crack growth rate for the perfectly straight crack path is known and that everything else is held fixed. As mentioned above, the fatigue cracks in nc Ni can be approximated as being perfectly straight (Fig. 11c,f). Therefore, the crack growth rate of the ufc Ni can be estimated by assuming the rate of growth in the nc Ni is tantamount to the linear (undeflected) growth rate, $(da/dN)_L$. The mismatch parameter, χ, is then varied to gage the level of shift in the overall fatigue crack growth rate under each loading condition.

Fig. 12 illustrates the crack growth trends predicted from the nc Ni data, superimposed on the data from Fig. 5. A reference curve for an ideally elastic periodically deflected crack ($\chi=0$) is plotted in each case. The magnitude of χ needed to match the experimental observations decreases from 0.08 for $R=0.1$ to 0.04 for $R=0.7$. This is consistent with expectations since fracture surface separation increases with load ratio R. Furthermore, these values of χ are approximately on the order of values observed for aluminum alloys subjected to in-situ fatigue crack growth experiments inside the scanning electron microscope [37]. The $\chi=0$ curves in the figure indicate that the contribution of the deflection term alone [$D\cos^2(\theta/2)$] is limited, relative to the combined effects of fracture surface mismatch ($\chi>0$) and the purely geometric consequences of Eq. (10). Correspondingly, errors associated with the finite size of the kinked crack with respect to the plastic zone size are also limited. Deviation from the predicted crack growth rate at high levels of applied loading is expected since the crack tip opening displacement, and therefore the changes in effective crack driving force for fatigue fracture, are not constant, but are rather dependent upon the loads applied. In addition, increased ΔK levels are accompanied by increased crack tip plasticity. When the plastic zone size encompasses many grains, multiple slip dominates, resulting in a more planar Stage II [38] crack growth. The experimental data is therefore expected to approach that for a linear undeflected crack at elevated levels of applied loading. This was indeed observed in the electrodeposited Ni system (Fig. 12).

The trends emerging from the results described above for electrodeposited nc and ufc Ni are also broadly applicable to the case of pure Ti, where grain refinement in the ufc range is achieved through a very different processing route, i.e. ECAP. Fig. 13 illustrates the level of crack path tortuosity in both the mc and ufc Ti, under similar loading conditions. As was the case with Ni, the ECAP ufc Ti exhibits a comparatively straight crack path, relative to its mc counterpart. The reduction in effective driving force for crack propagation in the mc material is again assumed to result from a combination of crack deflection and asperity contact. This can also be substantiated by the sensitivity to the load ratio of the two materials. While the ufc Ti exhibits relatively less sensitivity to R (Fig. 10), the mc Ti shows a clear shift in the entire da/dN vs. ΔK curve as R is decreased from 0.3 to 0.1, indicating deflection and its attendant effects are more prevalent in the coarser grain material.

Assuming the ufc Ti fatigue crack does not deviate from the pure mode I growth plane, the results in Eqs. (9) and (10)

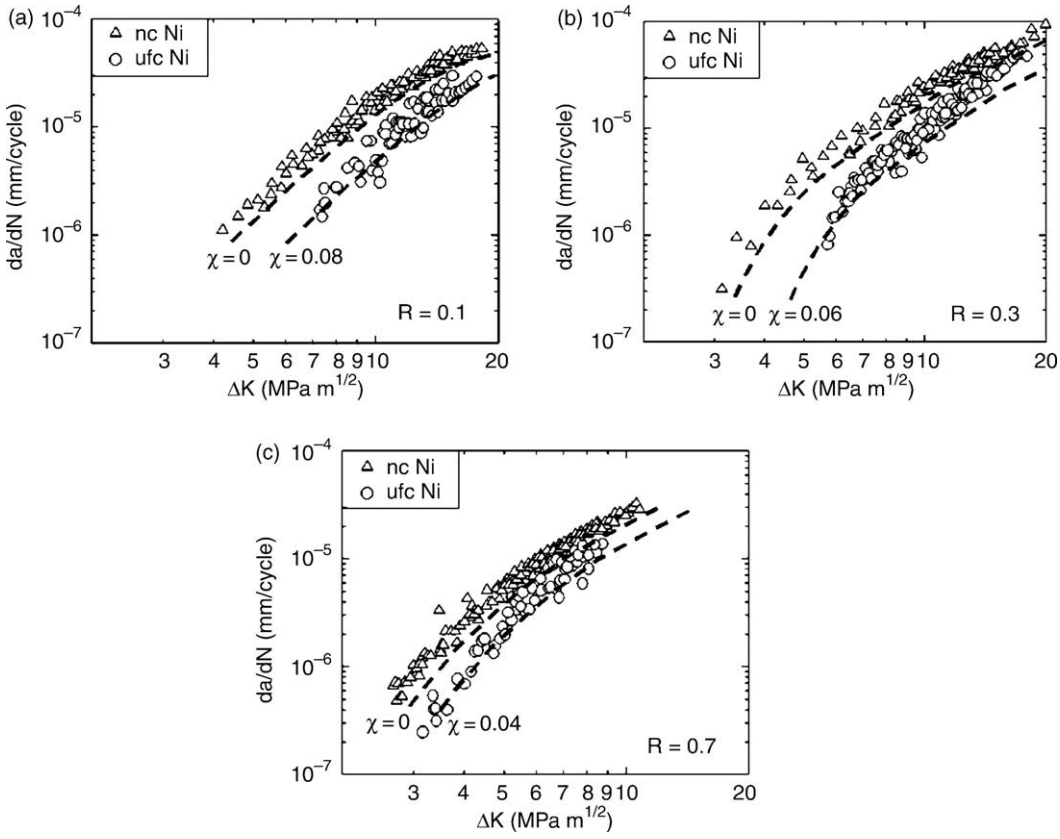

Fig. 12. Fatigue crack growth trends (depicted as broken lines) predicted from the crack deflection model described in [7], superimposed on the data from Fig. 5. The nc Ni growth rate is assumed tantamount to $(da/dN)_L$ in Eq. (10). A reference curve for an ideally elastic periodically deflected crack ($\chi = 0$), which sustains no premature crack face contact, is plotted in each case.

can be applied to assess the effect of crack deflection in mc Ti. Fig. 14 illustrates the upper and lower bounds of the mismatch parameter, χ, for $R = 0.1$ and 0.3. In the near-threshold, $\chi = 0.5$ most accurately captures the observed behavior. At sufficiently high levels of applied loading, large crack tip opening displacements and Stage II crack growth dominate, significantly reducing the extent of crack deflection in mc Ti. Accordingly, its crack growth rate approaches that of the ufc Ti at elevated ΔK levels. These trends of grain size effects on fatigue fracture mirror those observed in the electrodeposited Ni system.

The discussion up to this point has mainly explored the consequences of crack path changes, induced by differences in grain size and the associated alterations to fatigue crack growth mechanisms, on the overall subcritical fracture response. It is possible that other factors which are not considered up to this point, such as the effects of environment, could also influence the fatigue crack growth behavior. To explore the possible significance of such mechanisms, we consider the two-parameter characterization of crack growth based on a critical value of ΔK and K_{max} at each growth rate [39,40]. With this approach, fatigue threshold data, for a fixed crack growth rate, typically show an L-shaped curve (as seen in the lower Fig. 8), where ΔK^* and K^*_{max} represent the threshold values of alternating and maximum stress intensity factor values, respectively, to advance the crack at that growth rate. A plot of ΔK^* versus K^*_{max} over the entire range of fatigue crack growth rates is shown in Fig. 15 for the present nc and ufc Ni. Here, the solid line representing $\Delta K^* = K^*_{max}$ denotes purely mechanical fatigue fracture which is devoid of any influence from the environment or mechanistic factors by which a static mode of failure is introduced during fatigue fracture. Points A′ and C′ for the ufc Ni correspond to

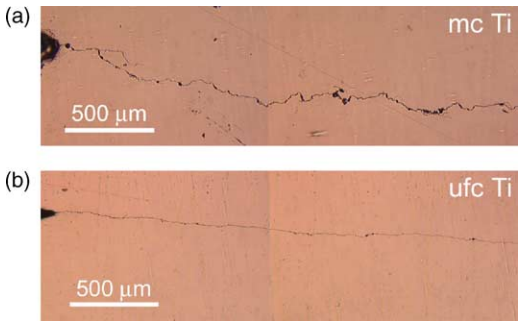

Fig. 13. Illustration of the crack path tortuosity in (a) commercially pure mc Ti subjected to an initial ΔK of 6.5 MPa $m^{1/2}$, and the lack thereof in (b) ufc ECAP Ti subjected to an initial ΔK of 5 MPa $m^{1/2}$. Each sample was loaded with a fatigue frequency of 10 Hz and load ratio of $R = 0.3$ at room temperature.

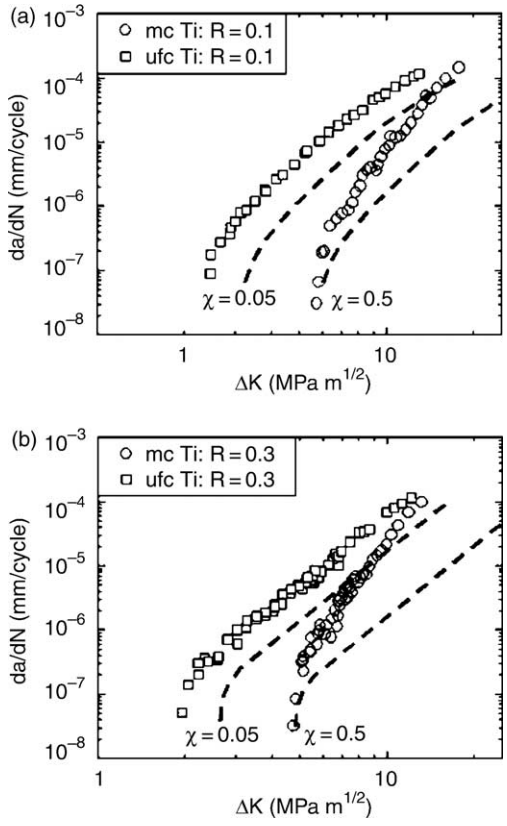

Fig. 14. Fatigue crack growth rate predictions, based on the deflection/closure model defined in [7], for commercially pure mc Ti at load ratios of (a) $R=0.1$ and (b) $R=0.3$. Crack growth data for the ufc ECAP Ti is assumed to correspond to the linear undeflected growth rate in Eq. (10).

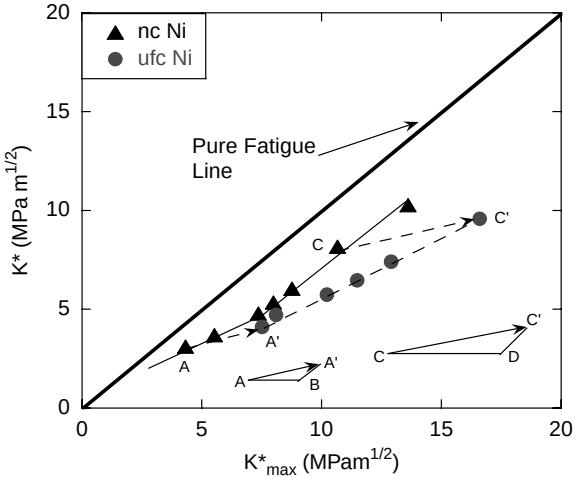

Fig. 15. A plot of ΔK^* versus K^*_{max} over the entire range of fatigue crack growth for nc and ufc Ni. Points A′ and C′ for the ufc Ni correspond to the same growth rates as points A and C for the nc Ni. Thus, vectors AA′ or CC′ represent additional driving forces needed to accomplish the same da/dN in ufc Ni as in nc Ni. These vectors can be further resolved into purely cyclic (or mechanical fatigue) components, BA′ or DC′, and purely static components, AB or CD, which are possibly associated with environmental or other effects.

the same growth rates as points A and C for the nc Ni. Thus vectors AA′ or CC′ represent additional driving forces needed to accomplish the same da/dN in ufc Ni as in nc Ni. These vectors can be further resolved into purely cyclic (or mechanical fatigue) components, BA′ or DC′, and purely static components, AB or CD, which are possibly associated with environmental effects or other unknown effects. It is evident from Fig. 15 that ufc Ni exhibits a relatively stronger propensity for static mode effects during fatigue fracture. The origins of such grain size induced differences are presently unknown and require further detailed investigation.

5. Conclusions

The effects of grain size, spanning the nano- to the microcrystalline regimes, on the fatigue behavior of metals were investigated. Grain refinement in the nc and ufc regimes has been shown to have a substantial effect on stress-controlled fatigue life, as well as the fatigue crack growth behavior. Specifically, crack growth results obtained in electrodeposited, fully dense pure Ni indicate that grain refinement in the nc regime can have a deleterious effect on the resistance to subcritical fatigue fracture. On the other hand, a beneficial effect of grain size reduction was observed with respect to the total life under stress-controlled fatigue.

The observed effects of grain size on fatigue crack growth rates are accompanied by a corresponding systematic change in which crack path and fracture surface features evolve during subcritical fatigue crack growth. Specifically, grain refinement from the mc to the ufc to the nc regime in pure Ni and from the mc to the ufc regime in pure Ti causes a concomitant smoothening of fracture surface features. A crack deflection model was used to rationalize the apparent decrease in fatigue crack growth rate in coarser grained materials. Furthermore, the trends pertaining to the effects of grain size on fatigue fracture that were observed for electrodeposited materials also hold for fine-grained metals and alloys synthesized by other processing routes such as cryo-milling and ECAP. Some differences have also been identified in the manner which varying the grain size influences the extent of purely cyclic fatigue fracture in relation to possible contributions from static fracture modes or environmental factors.

Acknowledgements

This work was supported at the Massachusetts Institute of Technology by the Defense University Research Initiative on NanoTechnology on ‘Damage-Failure-Resistant Nanostructures and Interfacial Materials’ which is funded by the Office of Naval Research under Grant N00014-01-1-0808. The authors thank Dr. A. K. Vasudevan, Dr. K. Sadananda for many discussions on this work. The authors are grateful to

Prof. R.Z. Valiev, Dr. D.V. Gunderov of the Institute of Physics of Advanced Materials of the Ukranian Science Academy in Ufa, Russia, for their help in the preparation of the ECAP Ti specimens studied in this work.

References

[1] Suresh S. Fatigue of materials. 2nd ed. Cambridge: Cambridge University Press; 1998.
[2] Agnew SR, Weertman JR. Cyclic softening of ultrafine grain copper. Mater Sci Eng 1998;A244:145–53.
[3] Agnew SR, Vinogradov AYu, Hashimoto S, Weertman JR. Overview of fatigue performance of Cu processed by severe plastic deformation. J Electron Mater 1999;28:1038–44.
[4] Mughrabi H, Höppel HW. Cyclic deformation and fatigue properties of ultrafine grain size materials: current status and some criteria for improvement of the fatigue resistance. Mater Res Soc Symp Proc 2001;634:B2.1.1–B2.1.12.
[5] Hanlon T, Kwon Y-N, Suresh S. Grain size effects on the fatigue response of nanocrystalline metals. Scripta Mater. 2003;49:675–80.
[6] Pao P. Paper presented at this symposium, September 2004.
[7] Suresh S. Fatigue crack deflection and fracture surface contact: micromechanical models. Metall Trans A 1985;16A:249–60.
[8] Gleiter H. Nanostructured materials: basic concepts and microstructure. Acta Mater 2000;48:1–29.
[9] Arzt E. Size effects in materials due to microstructural and dimensional constraints: a comparative review. Acta Mater 1998; 46(16):5611–26.
[10] Gleiter H. Materials with ultrafine microstructures: retrospectives and perspectives. Nanostruct Mater 1992;1:1–19.
[11] Hahn H. Microstructure and properties of nanostructured oxides. Nanostruct Mater 1993;2:251–65.
[12] Kim Y-W, Bidwell LR. Effects of microstructure and aging treatment on the fatigue crack growth behavior of high strength P/M aluminum alloy X7091. In: Kiczak MJ, Hildeman GJ, editors. High-strength powder metallurgy aluminum alloys, 1982. p. 107–24.
[13] Kumar KS, Van Swygenhoven H, Suresh S. Mechanical behavior of nanocrystalline metals and alloys. Acta Mater. 2003;51:5743–74.
[14] El-Sherik AM, Erb U. Synthesis of bulk nanocrystalline nickel by pulsed electrodeposition. J Mater Sci 1995;30:5743–9.
[15] Koch CC. Synthesis of nanostructured materials by mechanical milling: problems and opportunities. Nanostruct Mater 1997;9:13–22.
[16] Fecht H-J. Nanostructure formation by mechanical attrition. Nanostruct Mater 1995;6:33–42.
[17] Inoue A. Fabrication and novel properties of nanostructured Al based alloys. Mater Sci Eng 1994;A179/A180:57.
[18] Gleiter H. Nanocrystalline materials. Prog Mater Sci 1989;33: 223–315.
[19] Lu K. Nanocrystalline metals crystallized from amorphous solids: nanocrystallization, structure, and properties. Mat Sci Eng 1996;R16: 161–221.
[20] Hanlon T. Grain size effects on the fatigue response of nanocrystalline materials. Ph.D. Thesis, Massachusetts Institute of Technology, Cambridge, MA; 2004.
[21] Wang Y, Jiang S, Wang M, Wang S, Xiao TD, Strutt PR. Abrasive wear characteristics of plasma sprayed nanostructured alumina/titania coatings. Wear 2000;237:176–85.
[22] Valiev RZ, Islamgaliev RK, Alexandrov IV. Bulk nanostructured materials from severe plastic deformation. Prog Mater Sci 2000;45: 103–89.
[23] Zhou F, Rodriguez R, Lavernia EJ. Thermally stable nanocrystalline Al–Mg alloy powders produced by cryomilling. Mater Sci Forum 2003;386–388:409–14.
[24] Han BQ, Lee Z, Nutt SR, Lavernia EJ, Mohamed FA. Mechanical properties of and ultrafine-grained Al–7.5%Mg alloy. Metall Mater Trans A 2003;34(3):603–13.
[25] Suresh S. Micromechanisms of fatigue crack growth retardation following overloads. Eng Fract Mech 1983;18(3):577–93.
[26] Christman T, Suresh S. Crack initiation under far-field cyclic compression and the study of short fatigue cracks. Eng Fract Mech 1986;23:953–64.
[27] Bloom JM. The short single edge crack specimen with linearly varying end displacements. Int J Fract 1967;3:235–42.
[28] Harris DO. Stress intensity factors for hollow circumferentially notched round bars, transactions of ASME J Basic Eng 1969;89: 49–54.
[29] Bowie OL, Freese CE. Cracked rectangular sheet with linearly varying end displacements. Eng Frac Mech 1981;14:519–26.
[30] Marchand N, Parks DM, Pelloux RM. K_I-solutions for single edge notch specimens under fixed end displacements. Int J Fract 1986;31: 53–65.
[31] Kumar KS, Suresh S, Chisholm MF, Horton JA, Wang P. Deformation of electrodeposited nanocrystalline nickel. Acta Mater 2003;51:387–405.
[32] Schwaiger R, Moser B, Dao M, Chollacoop N, Suresh S. Some critical experiments on the strain rate sensitivity of nanocrystalline nickel. Acta Mater 2003;51:5159–72.
[33] Stolyarov VV, Zhu YT, Alexandrov IV, Lowe TC, Valiev RZ. Influence of ECAP routes on the microstructure and properties of pure Ti. Mater Sci Eng 2001;A299:59–67.
[34] Shih CF. Relationships between the J-integral and the crack opening displacement for stationary and extending cracks. J Mech Phys Solids 1981;29:305–26.
[35] Bilby BA, Cardew GE, Howard IC. In: Taplin DMR, editor. Fracture, 3, 1977. p. 197–200.
[36] Cotterell B, Rice JR. Slightly curved or kinked cracks. Int J Fract 1980;16:155–69.
[37] Carter RD, Lee E-W, Starke Jr EA, Beevers CJ. The effect of microstructure and environment on fatigue crack closure of 7475 aluminum alloy. Metall Trans A 1984;15A:555–63.
[38] Forsyth PJE. A two stage process of fatigue crack growth. Crack propagation. Proceedings of Cranfield Symposium 1962, p.p. 76–94.
[39] Vasudevan AK, Sadananda K, Louat N. A review of crack closure, fatigue crack threshold and related phenomena. Mater Sci Eng A 1994;A188:1–22.
[40] Sadananda K, Vasudevan AK, Holtz RL. Extension of the unified approach to fatigue crack growth to environmental interactions. Int J Fatigue 2001;23:S277–S86.